Kiso Supernova Survey (KISS): Survey strategy

Tomoki MOROKUMA,[1,*] Nozomu TOMINAGA,[2,3] Masaomi TANAKA,[4]
Kensho MORI,[5] Emiko MATSUMOTO,[2] Yuki KIKUCHI,[1] Takumi SHIBATA,[2]
Shigeyuki SAKO,[1] Tsutomu AOKI,[6] Mamoru DOI,[1,7] Naoto KOBAYASHI,[1]
Hiroyuki MAEHARA,[6] Noriyuki MATSUNAGA,[8] Hiroyuki MITO,[6]
Takashi MIYATA,[1] Yoshikazu NAKADA,[1] Takao SOYANO,[6] Ken'ichi TARUSAWA,[6]
Satoshi MIYAZAKI,[4] Fumiaki NAKATA,[9] Norio OKADA,[4] Yuki SARUGAKU,[10]
Michael W. RICHMOND,[11] Hiroshi AKITAYA,[12] Greg ALDERING,[13]
Ko ARIMATSU,[8,10] Carlos CONTRERAS,[14,15] Takashi HORIUCHI,[16]
Eric Y. HSIAO,[14,15] Ryosuke ITOH,[5] Ikuru IWATA,[9] Koji S. KAWABATA,[12]
Nobuyuki KAWAI,[17] Yutaro KITAGAWA,[1] Mitsuru KOKUBO,[1] Daisuke KURODA,[18]
Paolo MAZZALI,[19,20,21] Toru MISAWA,[22] Yuki MORITANI,[12] Nidia MORRELL,[14]
Rina OKAMOTO,[16] Nikolay PAVLYUK,[23] Mark M. PHILLIPS,[14] Elena PIAN,[24,25]
Devendra SAHU,[26] Yoshihiko SAITO,[17] Kei SANO,[8,10] Maximilian
D. STRITZINGER,[15] Yutaro TACHIBANA,[17] Francesco TADDIA,[27]
Katsutoshi TAKAKI,[5] Ken TATEUCHI,[1] Akihiko TOMITA,[28] Dmitry TSVETKOV,[23]
Takahiro UI,[5] Nobuharu UKITA,[18] Yuji URATA,[29] Emma S. WALKER,[30]
and Taketoshi YOSHII[17]

[1]Institute of Astronomy, Graduate School of Science, The University of Tokyo, 2-21-1 Osawa, Mitaka, Tokyo 181-0015, Japan
[2]Department of Physics, Faculty of Science and Engineering, Konan University, 8-9-1 Okamoto, Kobe, Hyogo 658-8501, Japan
[3]Kavli Institute for the Physics and Mathematics of the Universe (WPI), The University of Tokyo, 5-1-5 Kashiwanoha, Kashiwa, Chiba 277-8583, Japan
[4]National Astronomical Observatory of Japan, 2-21-1 Osawa, Mitaka, Tokyo 181-8588, Japan
[5]Department of Physical Science, Hiroshima University, 1-3-1 Kagamiyama, Higashi-Hiroshima, Hiroshima 739-8526, Japan
[6]Kiso Observatory, Institute of Astronomy, Graduate School of Science, The University of Tokyo 10762-30, Mitake, Kiso-machi, Kiso-gun, Nagano 397-0101, Japan
[7]Research Center for the Early Universe, Graduate School of Science, The University of Tokyo, 7-3-1 Hongo, Bunkyo-ku, Tokyo 113-003, Japan
[8]Department of Astronomy, Graduate School of Science, The University of Tokyo, 7-3-1 Hongo, Bunkyo-ku, Tokyo 113-0033, Japan
[9]Subaru Telescope, 650 North A'ohoku Place, Hilo, HI 96720, USA
[10]Institute of Space and Astronautical Science, Japan Aerospace Exploration Agency, 3-1-1 Yoshinodai, Chuo-ku, Sagamihara, Kanagawa 252-5210, Japan
[11]Department of Physics, Rochester Institute of Technology, Building 76-1274, 85 Lomb Memorial Drive, Rochester, NY 14623-5603, USA
[12]Hiroshima Astrophysical Science Center, Hiroshima University, 1-3-1 Kagamiyama, Higashi-Hiroshima, Hiroshima 739-8526, Japan
[13]Lawrence Berkeley National Laboratory, 1 Cyclotron Road, Berkeley, CA 94720, USA
[14]Carnegie Observatories, Las Campanas Observatory, Colina El Pino, Casilla 601, Chile

[15]Department of Physics and Astronomy, Aarhus University, Ny Munkegade, DK-8000 Aarhus C, Denmark

[16]Department of Physics, Faculty of Science, Shinshu University, 3-1-1 Asahi, Matsumoto, Nagano 390-8621, Japan

[17]Department of Physics, Tokyo Institute of Technology, 2-12-1 Ookayama, Meguro-ku, Tokyo 152-8551, Japan

[18]Okayama Astrophysical Observatory, National Astronomical Observatory of Japan, 3037-5 Honjo, Kamogata, Asakuchi, Okayama 719-0232, Japan

[19]Astrophysics Research Institute, Liverpool John Moores University, IC2, Liverpool Science Park, 146 Brownlow Hill, Liverpool L3 5RF, UK

[20]Max-Planck Institut für Astrophysik, Karl-Schwarzschildstr. 1, D-85748 Garching, Germany

[21]INAF-Osservatorio Astronomico di Padova, Vicolo dell'Osservatorio 5, I-35122 Padova, Italy

[22]School of General Education, Shinshu University, 3-1-1 Asahi, Matsumoto, Nagano 390-8621, Japan

[23]Lomonosov Moscow State University, Sternberg Astronomical Institute, 13 Universitetskij prospekt, Moscow 119234, Russia

[24]Scuola Normale Superiore di Pisa, Piazza dei Cavalieri 7, I-56126 Pisa, Italy

[25]INAF-Istituto di Astrofisica Spaziale e Fisica Cosmica, Via P. Gobetti 101, I-40129 Bologna, Italy

[26]Indian Institute of Astrophysics, Koramangala, Bangalore 560 034, India

[27]The Oskar Klein Centre, Department of Astronomy, Stockholm University, AlbaNova, SE-10691 Stockholm, Sweden

[28]Faculty of Education, Wakayama University, Sakaedani 930, Wakayama 640-8510, Japan

[29]Institute of Astronomy, National Central University, Chung-Li 32054, Taiwan

[30]Department of Physics, Yale University, PO Box 208120, New Haven, CT 06520-8120, USA

*E-mail: tmorokuma@ioa.s.u-tokyo.ac.jp

Abstract

The Kiso Supernova Survey (KISS) is a high-cadence optical wide-field supernova (SN) survey. The primary goal of the survey is to catch the very early light of a SN, during the shock breakout phase. Detection of SN shock breakouts combined with multi-band photometry obtained with other facilities would provide detailed physical information on the progenitor stars of SNe. The survey is performed using a $2°.2 \times 2°.2$ field-of-view instrument on the 1.05-m Kiso Schmidt telescope, the Kiso Wide Field Camera (KWFC). We take a 3-min exposure in g-band once every hour in our survey, reaching magnitude $g \sim 20$–21. About 100 nights of telescope time per year have been spent on the survey since 2012 April. The number of the shock breakout detections is estimated to be of the order of 1 during our three-year project. This paper summarizes the KISS project including the KWFC observing setup, the survey strategy, the data reduction system, and CBET-reported SNe discovered so far by KISS.

1 Introduction

The variable sky has been intensively explored by wide-field surveys such as the Palomar Transient Factory (PTF: Rau et al. 2009; Law et al. 2009), the Catalina Real-Time Sky Survey (CRTS: Drake et al. 2009), the La Silla-QUEST Low Redshift Supernova Survey (Baltay et al. 2013), the Mobile Astronomical System of the TElescope-Robots (MASTER: Lipunov et al. 2004), the Panoramic Survey Telescope and Rapid Response System (Pan-STARRS1: Kaiser et al. 2002), the SkyMapper (Keller et al. 2007), the SDSS (Sloan Digital Sky Survey) Stripe 82 Supernova Survey (Frieman et al. 2008; M. Sako et al. 2008, 2014), and the Deep Lens Survey (DLS: Wittman et al. 2002), with each survey having

uniform data quality controlled systematically, especially during the last two decades. Some of the ground-based large-aperture and space telescopes have also utilized their deep imaging capabilities to explore transient phenomena within the scheme of their deep surveys (Sarajedini et al. 2003, 2006; Cohen et al. 2006; Morokuma et al. 2008; Villforth et al. 2010; Grogin et al. 2011; Koekemoer et al. 2011; Postman et al. 2012). All these projects were made possible by the recent development of large mosaiced-CCD imaging cameras. However, we still have little knowledge of fast transient objects whose time scales are shorter than a day, except for a few classes of objects (e.g., rapidly variable stars such as RR Lyrae). One of the most interesting phenomena in this time scale is the shock breakout of a supernova (SN). Although the existence of this phenomenon was theoretically predicted about 40 years ago (Klein & Chevalier 1978) and many SN surveys have been conducted, there are only three serendipitous detections so far (SN 2008D in NGC 2770 in X-ray, Soderberg et al. 2008; SNLS-04D2dc and SNLS-06D1jd in ultraviolet, Schawinski et al. 2008; Gezari et al. 2008) due to the short time scale: just a few hours. Shock breakouts are one of the brightest phenomena associated with SNe and are considered to be associated with every SN. Shock breakouts of SN explosions with hydrogen envelopes in particular are luminous in the optical and last for a few hours by virtue of the large radius of the progenitor star. They are expected to be a new tool for exploring the distant universe (Tominaga et al. 2011). In this paper, we show our new survey optimized for detecting nearby SN shock breakouts.

A new wide-field optical imager, the Kiso Wide Field Camera (KWFC: Sako et al. 2012), for the 1.05-m Kiso Schmidt telescope operated by the Institute of Astronomy of the University of Tokyo, in Nagano, Japan, was developed and has been open to public use since 2012 April, succeeding the former camera 2kCCD (Itoh et al. 2001). We started a high-cadence SN survey, called the Kiso Supernova Survey (KISS), with KWFC in 2012 April within the scheme of the Kiso Observatory Large Programs. Another program is a search mainly for periodic variable stars in the Galactic plane, called the KWFC Intensive Survey of the Galactic Plane (KISOGP). These programs are scheduled to be conducted until 2015 March.

The structure of this paper is as follows. We summarize the KISS observations including our observing strategy and the data reduction system in sections 2 and 3, respectively. Our initial results are shown in section 4. Section 5 is a summary of the paper. We use the standard ΛCDM cosmological parameters of $(H_0, \Omega_M, \Omega_\Lambda) = (71, 0.27, 0.73)$ (Komatsu et al. 2011). All magnitudes are measured in the AB system. All coordinates are measured in J2000.0 and all the dates are in UT.
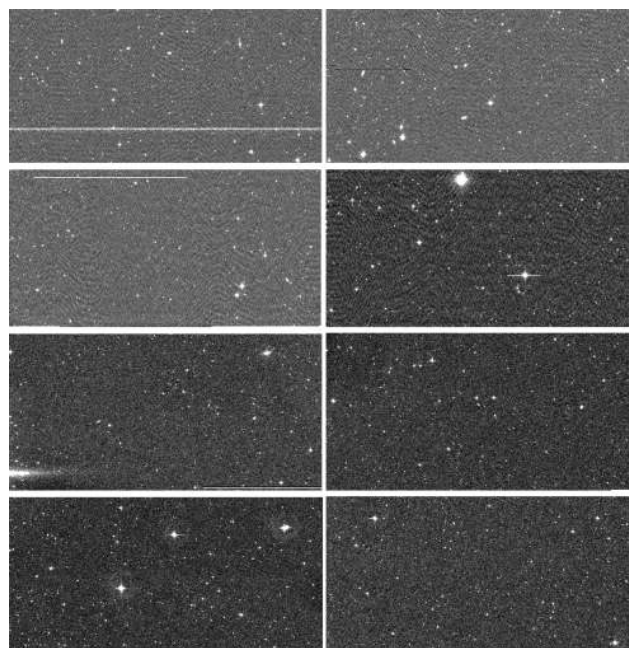

Fig. 1. An example of the entire KWFC FoV (1×1 binning, g-band, 300-s exposure). The top four CCDs are made by SITe and the bottom four CCDs those of MIT/LL. North is up and east is to the left. The gaps on sky are $82''$–$84''$ and $48''$–$62''$ in the north–south and east–west directions, respectively. There are some defects on the CCDs.

2 KISS observations

2.1 Kiso Wide Field Camera (KWFC)

The KWFC is an optical, wide-field, 64-megapixel imager attached to the prime focus of the Kiso Schmidt telescope covering $2°\!.2 \times 2°\!.2$ with four SITe and four MIT Lincoln Laboratory (MIT/LL) $15\,\mu\mathrm{m}$ $2\,\mathrm{k} \times 4\,\mathrm{k}$ CCDs (figure 1). The plate scale is $0''\!.946$ pixel^{-1} and the effective area is $4.6\,\mathrm{deg}^2$. KWFC is uniquely equipped with a filter exchanger based on an industrial robot arm and a magazine unit capable of storing 12 filters. For the KISS observations, we adopt 1×1 binning (no binning) and SLOW (all eight chips) readout mode. All the CCDs are read out by the Kiso Array Controller (KAC: Sako et al. 2012). In this mode, the readout noise is about 20 and 5–10 electrons for the SITe and MIT/LL CCDs, respectively. The quantum efficiency of these CCDs is 40%–65% in the g-band used for the KISS observations. The readout time in total is 12.5 s including the wiping time. Typical telescope slewing time from field to field, which is usually finished during the readout, is about 2 min. In total, one typical 3-min exposure takes about 5–6 min and the observing efficiency is about 50%–60%. These parameters, as well as the survey strategy of KISS, are summarized in table 1.

Table 1. Summary of the KISS survey instrument and strategy.

Telescope	1.05-m Kiso Schmidt
Instrument	Kiso Wide Field Camera (KWFC)
Detector	Four MIT/LL CCDs and four SITe CCDs (15-μm pixel)
Field-of-view	$2°2 \times 2°2$
Pixel scale	$0''946$ pixel^{-1}
Effective area	4.6 deg^2
Pixel binning	1×1 (none)
Filter	g-band
Exposure time	180 s
Cadence	~ 1 hr
Survey field	SDSS fields with high star formation rates
Time allocation	~ 100 nights per year, around new moon

2.2 Kiso/KWFC observing set-up, filter selection, and cadence

The primary purpose of KISS is to catch the very early light of mainly core-collapse SNe, during the shock breakout phase, whose rising and declining time scales are as short as a few hours. The fact that there have been only three serendipitous detections of shock breakouts at other wavelengths (Soderberg et al. 2008; Schawinski et al. 2008; Gezari et al. 2008) indicates that the detection of shock breakouts requires a specially optimized high-cadence wide-field systematic survey. A successful survey must also have quick data reduction and quick follow-up observations for identification and characterization.

First, we conduct a single-band survey in g-band. Observations at short wavelengths are more effective in catching shock breakout light because the spectrum of the shock breakout can be approximated by quasi-blackbody radiation and the color temperature is of the order of 100000 K. Therefore, the spectral energy distribution (SED) peaks in the far-ultraviolet (far-UV) and the optical wavelength region is in the Rayleigh–Jeans regime: the flux density rapidly decreases with wavelength ($f_\lambda \propto \lambda^{-4}$). We choose g-band due to the higher total throughput of this band compared to the shorter-wavelength u-band. Secondly, we adopt a high cadence, as short as 1 hr, based on our detailed light curve simulations performed in subsection 2.4. As seen in subsection 2.4 and previous papers (Schawinski et al. 2008; Gezari et al. 2008), the time scales of the luminosity changes are as short as a few hours and observational information on this time scale would be important for deriving the physical parameters of shock breakout phenomenon.

KISS survey regions are selected from SDSS imaging fields where spectroscopic diagnostics for star formation rates are available (Brinchmann et al. 2004),[1] which are used to estimate the total star formation rates per KWFC field-of-view (FoV). The typical total star formation rate per KWFC FoV in our survey field is $\sim 20\,M_\odot$ yr^{-1} at $z < 0.03$. Archival images from the SDSS taken several years ago are used as reference images, since they are deeper and have higher spatial resolution than the KWFC images. Considering the seeing statistics in g-band at the Kiso site (typically $3''3$–$5''3$ FWHM at 20–80 percentile; $3''9$ FWHM at median), we adopt 1×1 binning in order to construct finely sampled point spread functions in the KWFC images for image subtraction with which transient and variable objects are isolated and located. We also choose the SLOW (all of the eight KWFC chips) readout mode to cover as wide an area as possible.[2]

In a typical case, we repeat a cycle which consists of one 3-min exposure for 20 different regions about five times per night. The depth of each image, defined as 50% detection completeness estimated by embedding artificial objects using IRAF/*artdata*, is $g \sim 20$–21 mag. The KISS detection limit matches the peak brightness of a typical shock breakout for a star of initial mass $20\,M_\odot$ and explosion energy $E = 1.0 \times 10^{51}$ erg at a distance of 160 Mpc (corresponding to $z \sim 0.04$), at which the SDSS spectroscopy completeness limit ($r < 17.7$) covers most of the populations of star-forming galaxies with supernova detection in the PTF (Arcavi et al. 2010).[3] In total, we observe about 100 deg^2 per night. The distribution of the number of epochs is shown in figure 2. A considerable number of fields have been visited in more than 100 epochs due to the high frequency of several visits per night. Under cloudy weather conditions, which provide shallower images up to $g < 19$, we change the strategy and observe several pointings for nearby galaxy clusters and groups.

---

[1] The MPA-JHU DR7 release of spectrum measurements. ⟨http://www.mpa-garching.mpg.de/SDSS/DR7/⟩.

[2] Other options for the binning and readout are 2×2 binning and FAST where only four MIT/LL CCDs are read out, respectively.

[3] The assumed maximum distance of $d = 160$ Mpc corresponds to a distance modulus $DM = 36.0$ mag; therefore, $r < 17.7$ mag corresponds to $M_r < -18.3$ mag. In Arcavi et al. (2010), most of the core-collapse SNe occur in galaxies brighter than this magnitude limit.
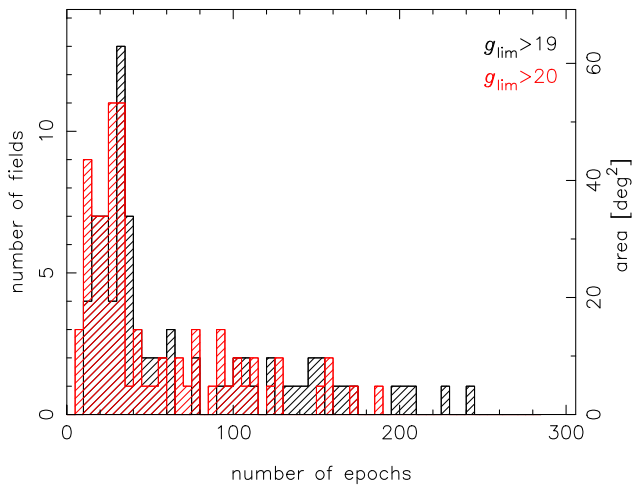
Fig. 2. The number of survey fields as a function of the number of the KISS observation epochs for different limiting magnitudes, $g_{lim} > 19$ mag in black and $g_{lim} > 20$ mag in red. (Color online)

About 100 nights per year (about 10 nights per month around new moon) are used for KISS observations; roughly half of them are shared with other science programs. Every year, from mid-June to mid-August, when the weather at the site is affected by the Japanese rainy season, the telescope and camera are under maintenance.

2.3 Follow-up observation strategy

Optical multi-band light curves are required to establish our physical understanding of a shock breakout (Tominaga et al. 2011) and thus it is important to launch follow-up imaging observations right after the discovery. When we find a candidate for a shock breakout after the procedure described in section 3 that includes quick automatic data reduction, image subtraction, candidate detection, and target screening, we trigger the Akeno 50-cm/MITSuME (Kotani et al. 2005; Yatsu et al. 2007; Shimokawabe et al. 2008) for simultaneous g'-, R_C-, and I_C-band automatic imaging observations for confirmation. The development of this automatic follow-up system is based on an automatic observation system originally developed for GRB (Gamma Ray Burst) optical afterglow follow-ups with MITSuME, which was completed in 2014 June. The MITSuME images, for which we do not perform image subtraction, are helpful if the SNe are spatially separated from the host galaxies or are on the diffuse host galaxies. When the candidate's existence is confirmed in MITSuME images with 9×1-min exposure or we judge the detection in the subtracted KWFC images are reliable, we quickly trigger multi-facility, multi-mode follow-up observations under the umbrella of the KISS collaboration. The collaborative follow-up observations so far include those with (in order of telescope aperture) the 50-cm MITSuME telescope

located at the Okayama Astrophysical Observatory (Yanagisawa et al. 2010), the 70-cm telescope of the Sternberg Astronomical Institute, KPNO 0.9-m, the Lulin One-meter Telescope (LOT), the Atacama Near-Infrared Camera (ANIR: Motohara et al. 2010; Konishi et al. 2015) on the 1-m miniTAO telescope (S. Sako et al. 2008; Minezaki et al. 2010), HOWPol (Kawabata et al. 2008) and HONIR (Sakimoto et al. 2012) on the 1.5-m Kanata telescope, the Kyoto Okayama Optical Low-dispersion Spectrograph (KOOLS: Yoshida 2005) on the Okayama 188-cm telescope, the Himalayan Faint Object Spectrograph (HFOSC) on the 2-m Himalayan Chandra Telescope (HCT), the Wide Field CCD Camera (WFCCD) on the Las Campanas 2.5-m du Pont telescope, the Andalucia Faint Object Spectrograph and Camera (ALFOSC) on the 2.5-m Nordic Optical Telescope (NOT), the Device Optimized for the LOw RESolution (DOLORES) on the 3.58-m Telescopio Nazionale Galileo (TNG: Barbieri 1997), the FoldedPort Infrared Echellette (FIRE) spectrograph on the 6.5-m Magellan Baade Telescope, and the Faint Object Camera And Spectrograph (FOCAS: Kashikawa et al. 2002) on the 8.2-m Subaru telescope.

2.4 Number estimate of supernova shock breakout detections and theoretical predictions

Based on the theoretical model of a shock breakout which succeeded in reproducing the UV light curve of the shock breakout and optical plateau multi-band light curves for SNLS-04D2dc (Tominaga et al. 2009), we optimize the KISS survey parameters as done in Tominaga et al. (2011) [see equation (3)] where they describe the expected performance of future large surveys with larger aperture telescopes. Whereas Tominaga et al. (2011) adopt the cosmic star formation history to derive expected numbers of shock breakouts up to $z \sim 3$, we first estimate the number of detections assuming a constant star formation rate density with redshift to evaluate how much observing time for a given star formation rate (i.e., directly translated to core-collapse SN rate) we need to detect a shock breakout. We here assume a detection limit of $g_{sub} = 19.8$ mag in our subtracted images, the typical depth as shown in subsection 3.2, for calculating the effective volume. We simulate light curves with various observation strategies; different cadence (time interval between exposures for a given field t_{int}, 0.5–2 hr), and different numbers of exposures per night N_{visit} (3–5) (i.e., different number of the fields N_{field} within a fixed observing time). In this paper, the detection of shock breakouts is defined so that the object is detected in one or more epochs around the shock breakout peak ($-0.1 < t < 0.1$ d, where t is measured relative to the peak)
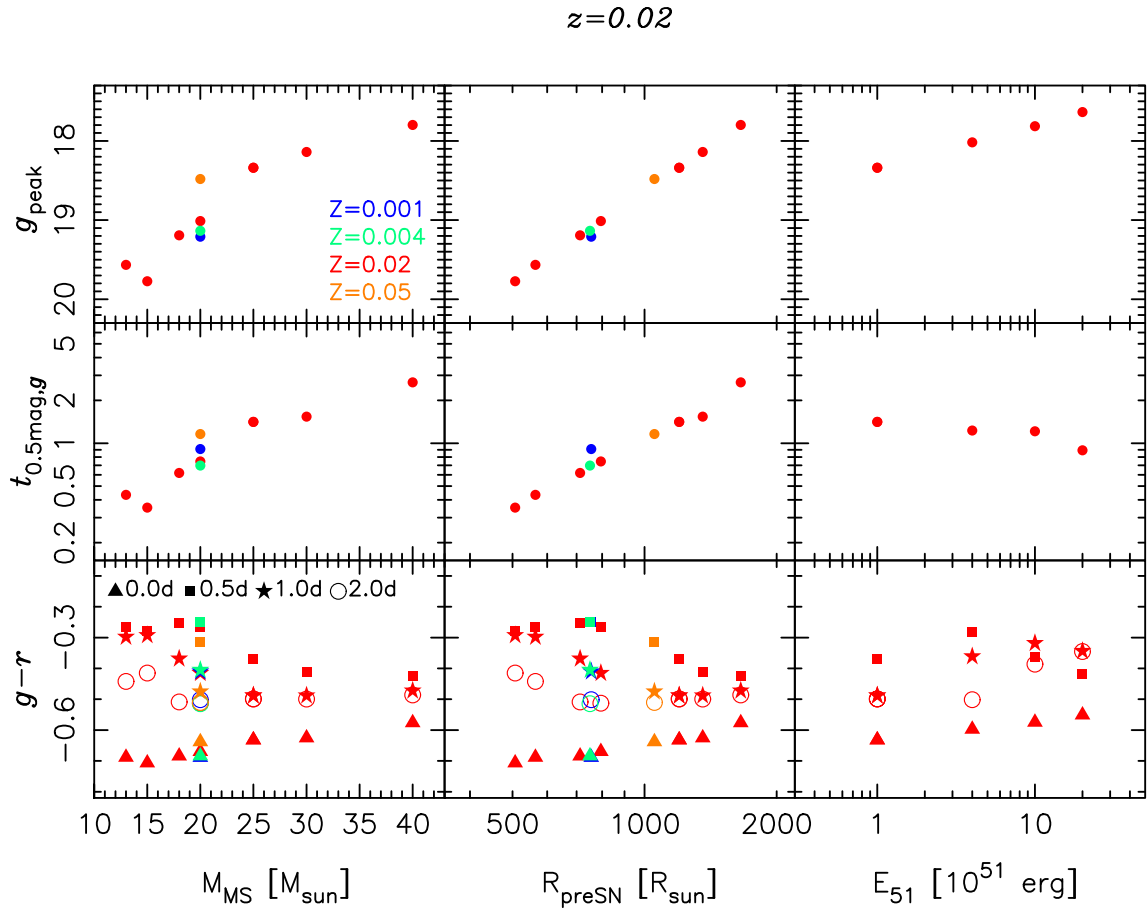
$$z = 0.02$$

Fig. 3. The dependency of observational quantities, peak g-band magnitude $m_{g,\mathrm{peak}}$, hours for 0.5 mag decline from the peak in g-band $t_{g,0.5\mathrm{mag}}$, and $g - r$ at $z = 0.02$ for different model parameters; main-sequence masses $M_\odot$, pre-supernova radius R_{preSN}, and explosion energies E_{51} from left to right. Main-sequence mass $M_\odot$ in the three right-hand panels are $25\,M_\odot$. Different colors indicate different metallicity; $Z = 0.001$, 0.004, 0.02, and 0.05 in blue, green, red, and orange, respectively. Different symbols (filled triangles, boxes, stars, and open circles) also indicate different epochs; $t = 0.0$, 0.5, 1.0, and 2.0 d from the time with the bluest $g - r$ color, slightly after the g-band peak. (Color online)

and in three or more epochs over a wider time range that includes the plateau phases. As a result, it is shown that the number of detections per unit star formation rate is 20%–50% larger for longer time interval t_{int} and the total number of detection per night is only 20% larger in the $N_{\mathrm{visit}} = 3$ case than that in the $N_{\mathrm{visit}} = 5$ case. We also estimate the observable redshift for each different survey strategy and find that about half of the detections are located at $z < 0.02$ and 90% of them are at $z < 0.03$ in every observation strategy.

It is important to enhance not only the number of the detected objects but also the number of the detected exposures for individual objects to identify the shock breakouts and characterize the progenitor stars. The top two rows of figure 3 show the dependencies of observational quantities on the theoretical model parameters; a brighter peak luminosity and slower decline rate of the shock breakout result from a progenitor star with a larger pre-supernova radius, i.e., higher main-sequence mass. Although

core-collapse SNe usually explode in dusty environment and are obscured by dust, some of the observational properties (e.g., decline rate) are free from dust extinction. Therefore, we conclude that the survey parameters as described in subsection 2.2, i.e., 1-hr cadence ($t_{\mathrm{int}} = 1$ hr) and five visits per night ($N_{\mathrm{visit}} = 5$) using a single g-band, which corresponds to 20 fields ($N_{\mathrm{field}} = 20$), would be the optimum strategy. In this survey parameter set, the expected number of shock breakout detections is an order of 1 during the three-year project term, considering all the factors described above and the typical SFR per KWFC FoV is $20\,M_\odot\,\mathrm{yr}^{-1}$ at $z < 0.03$.

Figure 4 shows simulated KWFC g-band light curves for shock breakouts of stars with $M = 15$, 20, and $30\,M_\odot$ at a distance of $d = 85$ Mpc ($z \sim 0.02$) by assuming the typical depth ($g_{\mathrm{sub}} = 19.8$ mag, $5\,\sigma$) and observing strategy of our survey. The figure demonstrates that the decline of the light curve after the shock breakout can be well characterized by our survey strategy. While the light curves are almost
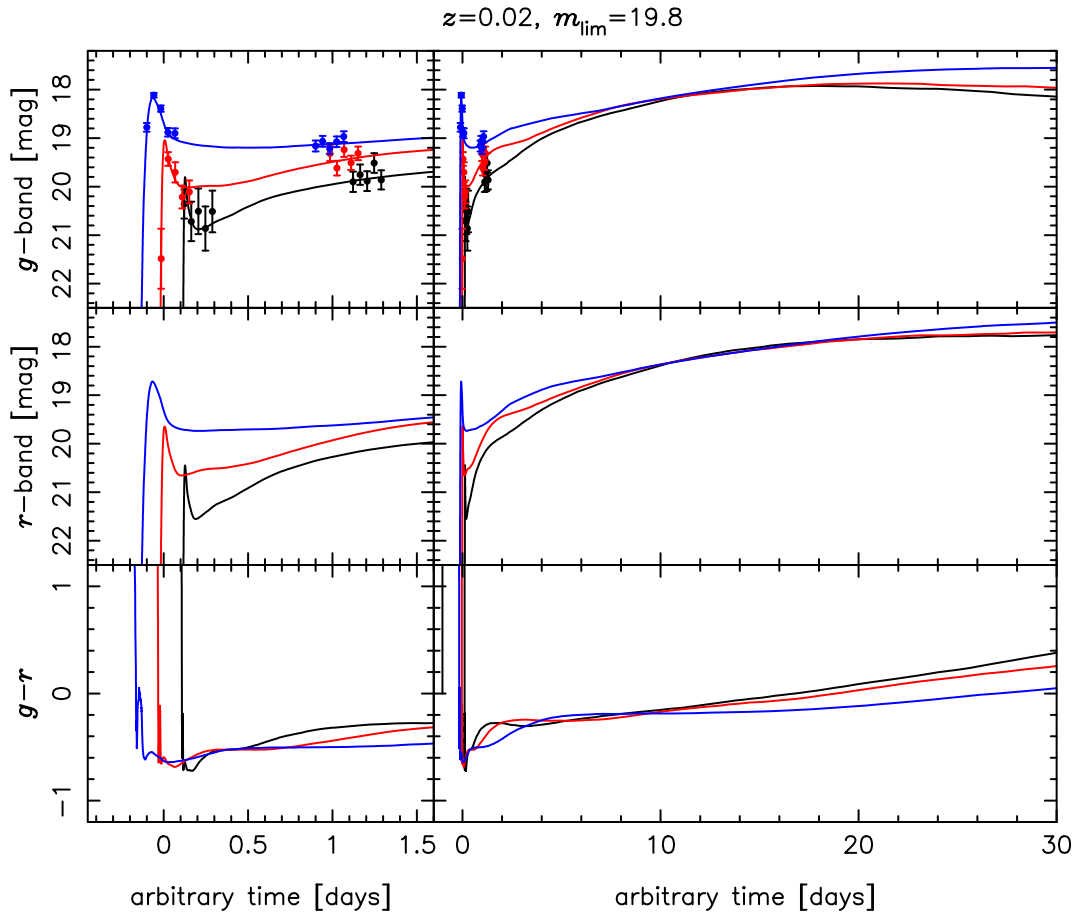
Fig. 4. Simulated g-band light curves for $M = 15$ (black), 20 (red), and 30 $M_\odot$ (blue) progenitor stars at $z = 0.02$ (at a distance of ~ 85 Mpc). Time in x-axis is arbitrarily shifted for ease of comparison. Photometric errors are calculated by assuming a limiting magnitude (5σ) of 19.8 mag. The left-hand panels are magnified views of the right-hand panels around the shock breakout phases. (Color online)

constant on the second day, the SNe brighten with time again and the luminosities in g-band peak at 20–30 d after the explosion (figure 4). The g-band and r-band magnitudes at the plateau phase are expected to be as bright as < 18 mag at $z = 0.02$. The plateau duration and the brightness and photospheric velocity at the plateau phase also depend on the pre-supernova radius, envelope mass, and explosion energy (Eastman et al. 1994) and have been frequently used to constrain the explosion properties (Utrobin & Chugai 2009). Therefore, in order to confirm the detection of the shock breakout and verify the constraints derived from the observational properties of the shock breakout, it is important to continuously observe the same fields over several months.

Further constraints on physical properties of shock breakouts discovered by KISS would be achieved with the quick follow-up observations described in subsection 2.3. For example, the change in time of observed colors such as $g - r$ in the shock breakout phase is also sensitive to the progenitor mass, as shown in the bottom row of figure 3. The color evolution indicates the photospheric temperature

and constrains the evolution of the photospheric radius, i.e., the shock velocity. This additional information determines the pre-supernova radius and the explosion energy independently. Furthermore, if spectroscopic observations are performed, growing metal absorption lines due to the decrease of the photospheric temperature will be observed (Gezari et al. 2008). The spectral evolution provides another clue to properties of shock breakouts and supernovae, e.g., pre-supernova radius, circumstellar material structure, and mass loss at the last stage of stellar evolution. It also reveals the structure of a radiation-mediated shock, in which radiation and matter are marginally coupled. This can test radiation hydrodynamics theories at high temperature, e.g., how the absorptive and scattering opacities contribute to the total opacity (Blinnikov et al. 2000).

3 Data reduction and transient detection

Here we summarize the data analysis procedure optimized for the KISS/KWFC data. Shock breakout is very rare and the time scale is as short as hours. It is essential to

find good candidates with high completeness and a low contamination rate from a huge amount of data as soon as possible, ideally automatically.

3.1 Automatic real-time data reduction

Data reduction starts automatically just after KWFC data are acquired. First, a standard reduction which includes overscan subtraction, overscan region trimming, bias subtraction, flat-fielding, and background subtraction is performed for each image. The bias and flat-field data used here are prepared before the night observations start. Then, astrometric solutions are also automatically obtained, with the USNO-B1.0 catalogue[4] adopted as the reference list, using the Optimistic Pattern Matching (OPM) algorithm (Tabur et al. 2007) implemented by one of the authors (NM). Typically 100–200 stars in the USNO-B1.0 catalogue are identified within each chip in our KISS observations (g-band, 180-s exposure, not in the Galactic plane) and used to obtain a linear transformation from the pixel coordinate to the celestial coordinate. The rms residual is about 0″.3 in both RA and Dec directions. Finally, calculations of the zeropoint magnitude and limiting magnitude (50% detection completeness magnitude) are done using the SDSS photometric catalog. These procedures are performed for each chip individually. It typically takes about 5 min to finish these procedures for each exposure (all eight chips).

3.2 Real-time transient detection

SDSS archival g-band images taken several years before the KWFC observations are used as reference images for image subtraction. The SDSS images are always deeper (g ∼ 22.2 mag, 95% detection repeatability for point sources) and sharper [∼ 1″.4 point source function (PSF) width in r-band according to the SDSS DR8 website[5]] with finer spatial sampling of 0″.396 pixel^{-1}, compared to the KWFC images (20–21 mag limit, 3″.3–5″.3 PSF FWHM, and 0″.946 pixel^{-1}). Transmission curves of the g-bands of these two datasets (SDSS and KWFC) are slightly different but this difference does not significantly affect the quality of image subtraction, although we need to take care of objects with extreme colors, i.e., steep spectrum in the g-bands.

Our transient detection pipeline performs the following procedures. First, cosmic rays are removed from the reduced KWFC data using the publicly available code, *L.A.Cosmic*[6]
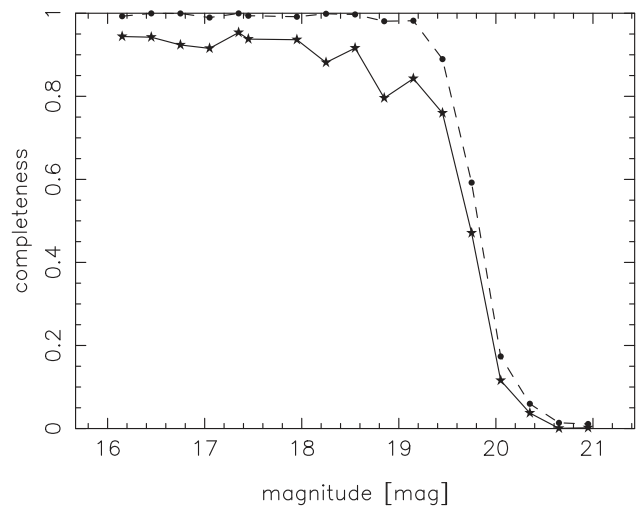

Fig. 5. Detection completeness as a function of magnitude estimated by embedding artifical sources in the KWFC images with 5σ detection limit of 20.5 mag. Dashed and solid lines show the completeness before and after screening (based on position, FWHM, and elongation). The missed fraction of real sources is about 10% as we adopt relatively stringent thresholds to achieve realtime detection of fast transients and to avoid too many spurious detections.

developed by van Dokkum (2001). The SDSS images prepared in advance are transformed to the KWFC images with *wcsremap*,[7] and then subtracted from the KWFC image using *hotpants*.[8] In the subtracted images, we search only for positive residuals with > 5σ detections using the *SExtractor* software (Bertin & Arnouts 1996). In this way, we obtain transient candidate catalogs about 10 minutes after the data acquisition.

Each exposure typically gives about 1000–1500 positive detections in the subtracted image. However, as in other transient surveys using image subtraction techniques, non-astrophysical sources always overwhelm the real sources (Bloom et al. 2012; Brink et al. 2013). Non-astrophysical sources include cosmic rays that are not removed by *L.A.Cosmic*, extended features around very bright saturated stars, and bad subtractions due to a misalignment of the images. To screen out these false detection, we first exclude the sources around bright, saturated stars and at the edges of the images. Next, we apply criteria based on the FWHM and elongation of the detected sources. Using these screening procedures, we reduce the number of candidates down to 10–50 per exposure. Even after this screening, there are still false detections, but the numbers of non-astrophysical and astrophysical sources are roughly comparable. The false positive rate (the fraction of non-astrophysical sources that are judged to be real objects) of our pipeline is about 1%–5%.

[4] ⟨https://tdc-www.harvard.edu/catalogs/ub1.html⟩.

[5] ⟨https://www.sdss3.org/dr8/scope.php⟩.

[6] ⟨http://obswww.unige.ch/∼tewes/cosmics_dot_py/⟩.

[7] ⟨http://www.astro.washington.edu/users/becker/v2.0/wcsremap.html⟩.

[8] ⟨http://www.astro.washington.edu/users/becker/v2.0/hotpants.html⟩.

Table 2. List of supernovae discovered and identified by KISS and reported to CBET except for SN 2014bk.

CBET name	SN type	Best match	z	t_{disc}	t_{spec}	m_{disc}	M_{peak}	Disc. date	Spec. date	References*
SN 2012cm	Ia	SN 2002hu	0.028	−8	−4	16.7	−19.2	2012/05/13.6	2012/05/17.5	[1],[2]
SN 2012cq	IIP	SN 2004et	0.026	−5	+6	17.4	−17.9	2012/05/13.5	2012/05/24.9	[3],[4]
SN 2012ct	IIP	SN 2005cs	0.039	−2	0	19.4	−16.8	2012/05/22.5	2012/05/24.9	[5],[6]
SN 2013I	IIP	SN 2005cs	0.035	+1	+5	18.7	−17.1	2013/01/11.4	2013/01/15.9	[7],[8]
SN 2013J	Ic	SN 1994I	0.034	−3	−2	18.7	−16.9	2013/01/19.8	2013/01/21.2	[9],[10]
SN 2013Y	Ia	SN 2005cf	0.077	0	+5	18.6	−18.9	2013/02/06.6	2013/02/11.2	[11],[12]
SN 2013al	Ia	SN 2006cf	0.132	0	+4	19.3	−19.6	2013/03/03.4	2013/03/07.1	[13],[14]
SN 2013ba	Ia	SN 1997bp	0.08†	−5	−3	19.2	−18.7	2013/04/06.7	2013/04/07.2	[15],[16]
SN 2014Q	Ia	SN 2002he	0.046	−11	−3	18.9	−18.3	2014/01/29.4	2014/02/06.0	[17],[18]
SN 2014S	IIP	SN 1999gi	0.04†	−8	−4	18.6	−18.2	2014/02/21.5	2014/02/25.1	[19],[20]
SN 2014T	IIn	SN 1996L	0.09†	+5	+8	18.7	−19.2	2014/02/22.7	2014/02/25.2	[21],[22]
SN 2014U	II	SN 2013hj	0.018	+17	+21	18.4	−16.4	2014/02/23.5	2014/02/27.2	[23],[24]
SN 2014an	Ia	SN 1984A	0.060	−8	−6	18.6	−18.7	2014/03/31.7	2014/04/02.7	[25],[26]
SN 2014bd	IIP	SN 2005cs	0.029	0	+13	20.2	−15.5	2014/04/23.6	2014/05/06.3	[27],[28]
SN 2014bo	Ia	SN 2004L	0.133	−11	−3	19.1	−20.0	2014/05/19.7	2014/05/27.5	[29],[30]

*References are [1] Morokuma et al. (2012a), [2] Itoh et al. (2012), [3] Morokuma et al. (2012b), [4] Walker et al. (2012a), [5] Morokuma et al. (2012c), [6] Walker et al. (2012b), [7] Tanaka et al. (2013a), [8] Stritzinger et al. (2013a), [9] Tanaka et al. (2013b), [10] Taddia et al. (2013a), [11] Tanaka et al. (2013c), [12] Taddia et al. (2013b), [13] Morokuma et al. (2013), [14] Walker et al. (2013), [15] Matsumoto et al. (2013), [16] Stritzinger et al. (2013b), [17] Morokuma et al. (2014a), [18] Walker et al. (2014a), [19] Tanaka et al. (2014a), [20] Walker et al. (2014b), [21] Tanaka et al. (2014b), [22] Walker et al. (2014c), [23] Tanaka et al. (2014c), [24] Hsiao et al. (2014), [25] Tominaga et al. (2014a), [26] Tanaka et al. (2014d), [27] Tominaga et al. (2014b), [28] Morrell et al. (2014), [29] Tominaga et al. (2014c), [30] Tanaka et al. (2014e).
†These redshifts are obtained by fitting the SN spectra.

Table 3. List of spectroscopic observations for the SNe reported to CBET except for SN 2014bk.

Telescope	Instrument	Slit width	Grism	R	λ range [Å]	t_{exp} [s]
Kanata	HOWPol	2.2	420 l/mm	400	4500–9000	300 × 6 (SN 2012cm)
TNG	DOLORES	1.5	LR-B	400	3500–8000	1200 × 2 (SN 2012cq, SN 2012ct, SN 2013al), 900 × 2 (SN 2014Q)
		1.0	LR-B	600	3500–8000	900 × 2 (SN 2014S), 1200 × 2 (SN 2014T)
NOT	ALFOSC	1.0	#4 300 l/mm	350	3500–8000	2400 × 1 (SN 2013I, SN 2013J, SN 2013Y, SN 2013ba)
Magellan	FIRE	0.6	prism	500	8100–24000	126.8 × 8 (SN 2014U)
OAO188	KOOLS	1.8	#5	500	4000–7400	1800 × 1 (SN 2014an), 1800 × 4 (SN 2014bo)
du Pont	WFCCD	1.65	Blue 400 l/mm	750	3800–9200	1500 × 2 (SN 2014bd)

We estimate the detection completeness of our pipeline by embedding artificial point sources in the KWFC images with *IRAF/artdata* and detecting them using the transient detection pipeline in exactly the same way as for the original images. Figure 5 shows a typical example of detection completeness as a function of magnitude. Detection completeness is about 0.9 after screening even for the bright sources, i.e., the fraction of real sources that are missed by our pipeline is about 10%. There is an inevitable trade-off between the false positive rate and the missed fraction (Bloom et al. 2012; Brink et al. 2013), and we adopt relatively stringent thresholds to achieve realtime detection of fast transients while avoiding too many spurious detections. For the same reason, the detection limit in the subtracted images is typically 0.5–1.0 mag shallower than that of the original images.

After running the transient detection pipeline, we list all the remaining candidates on a web page for visual inspection to further remove non-astrophysical sources and classify real objects. Real objects include not only SNe but also variable stars, active galactic nuclei (AGNs), and moving objects such as asteroids. For the classification, we cross-match the detected object catalog with quasar and AGN catalogs (Véron-Cetty & Véron 2010; Pâris et al. 2014), X-ray sources from ROSAT All-Sky catalogs [Bright Source Catalog (BSC), Voges et al. 1999; Faint Source Catalog (FSC)], the XMM serendipitous catalog (Watson et al. 2009), Chandra X-ray sources, the Minor Planet Checker (*MPChecker*),[9] and variable stars from SIMBAD. For rapid and efficient visual screening, we ask volunteer amateur

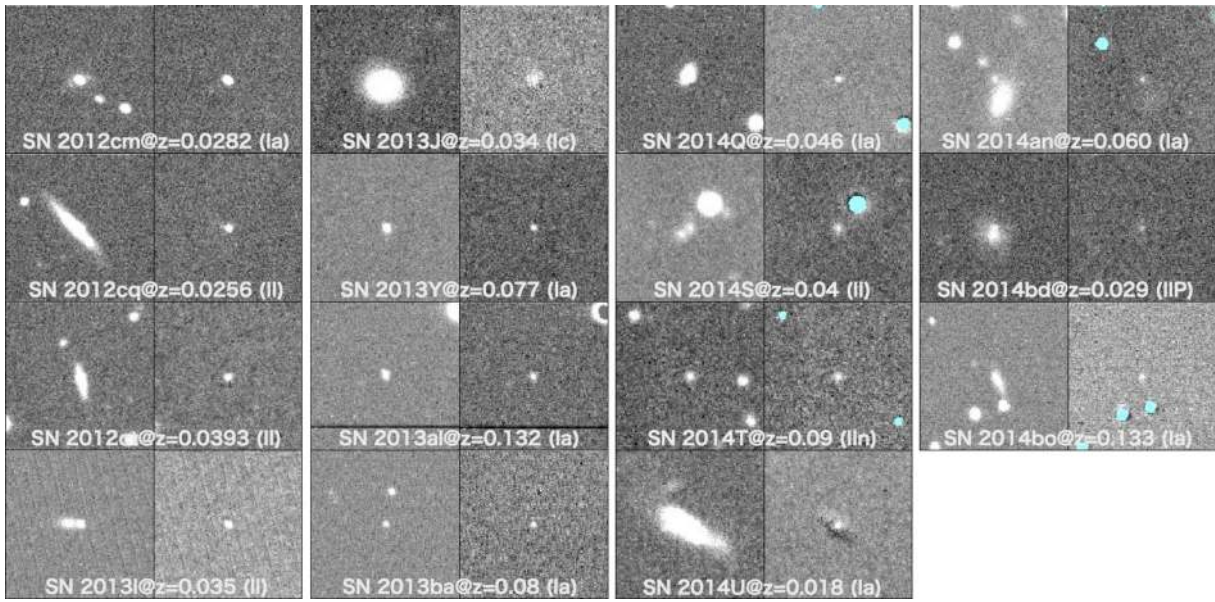[9] ⟨http://scully.cfa.harvard.edu/cgi-bin/checkmp.cgi⟩.

Fig. 6. Discovery images of the KISS SNe which were reported to CBET except for SN 2014bk. The image sizes are $2' \times 2'$. North is up and east is to the left. (Color online)
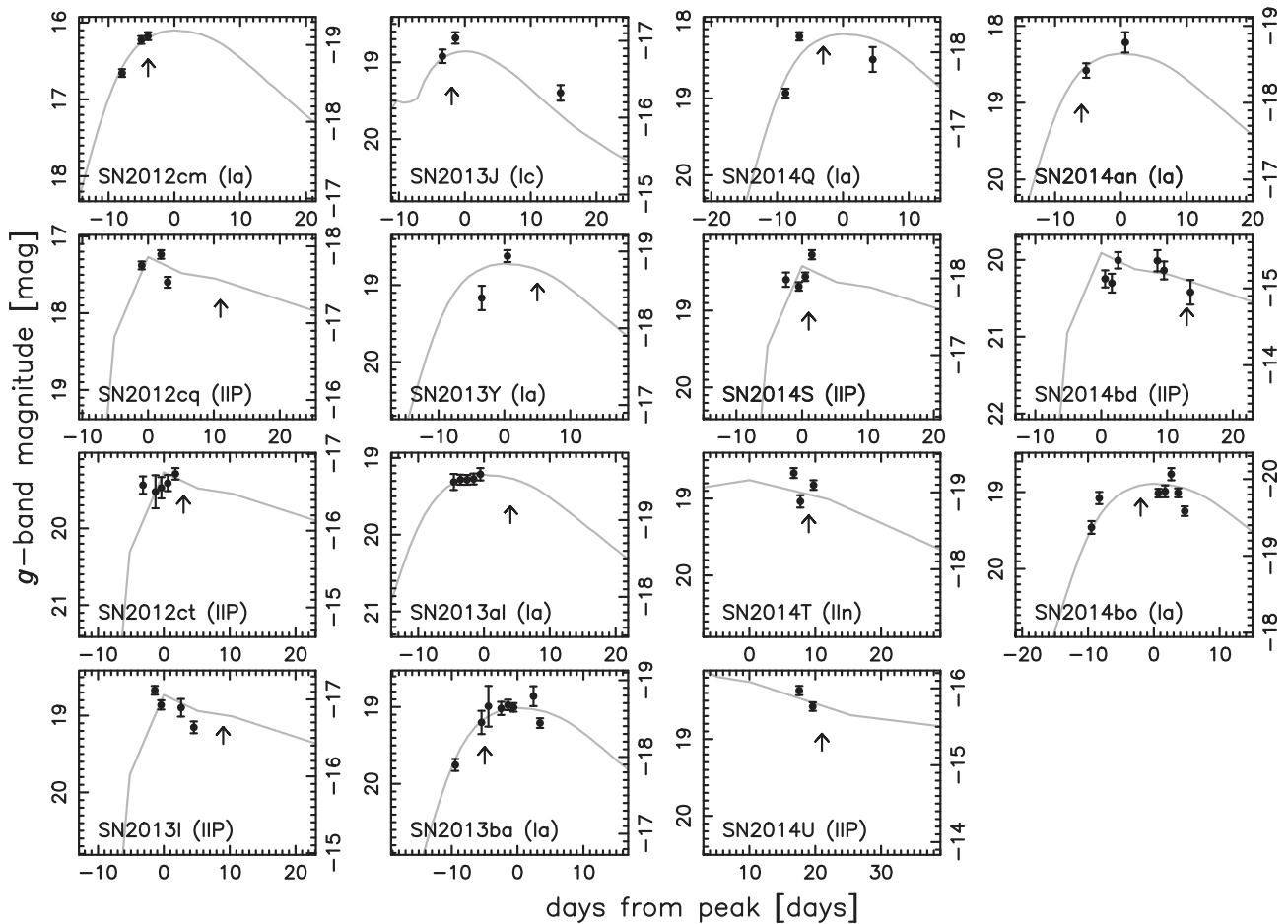

Fig. 7. Kiso/KWFC *g*-band light curves for the CBET-reported KISS SNe except for SN 2014bk. Nugent's light curve templates (Nugent et al. 2002) are overlaid in gray lines except for SN 2013J, for which Drout's SN Ic template (Drout et al. 2011) is used. Arrows indicate the dates of the spectroscopic observations. The right-hand *y*-axis indicates the absolute magnitude in *g*-band without *K*-corrections.
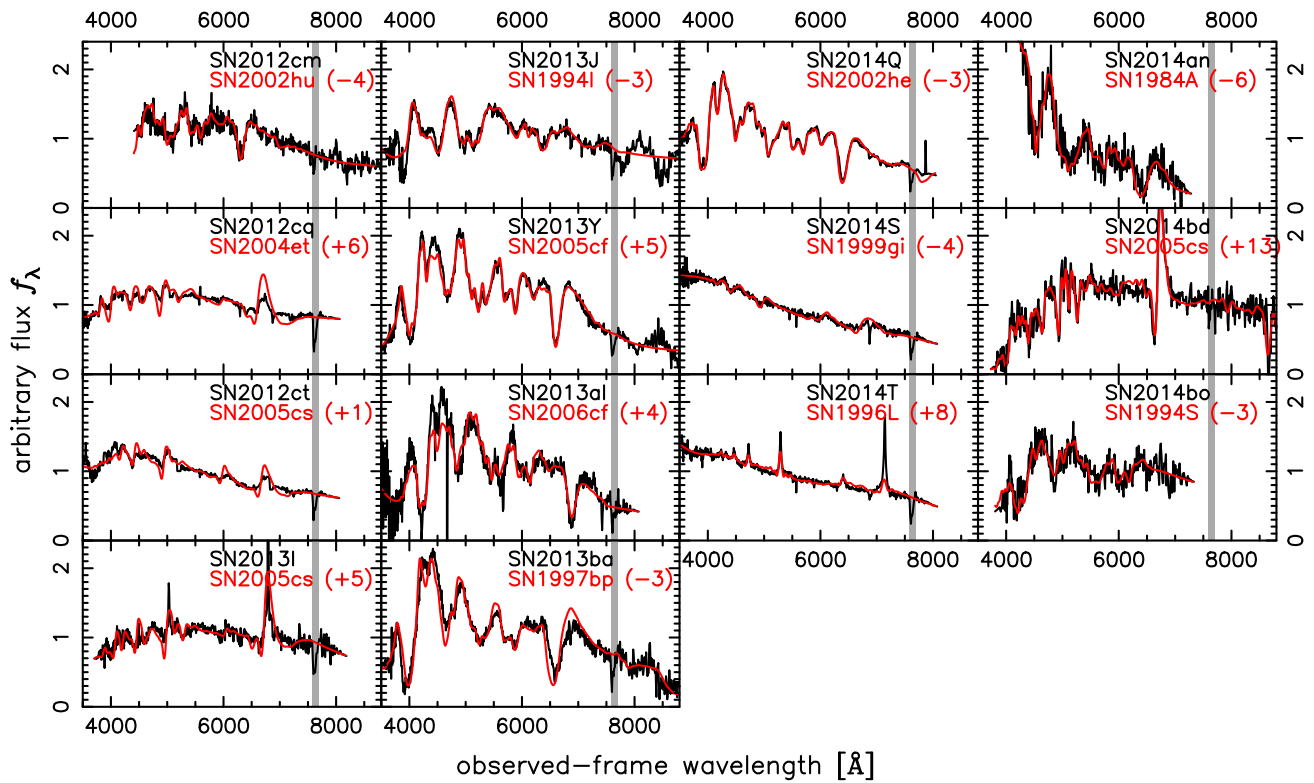
Fig. 8. Identification spectra for the CBET-reported KISS SNe except for SN 2014U (shown in figure 9) and SN 2014bk. The flux density (f_λ) scale has arbitrary units. Observed and template spectra are shown in black and red, respectively. SN spectra of the best-fitting templates are also shown in red characters with the estimated phase (days relative to max light) in parentheses. Telluric absorption wavelength regions around 7600 Å are gray-shaded. (Color online)
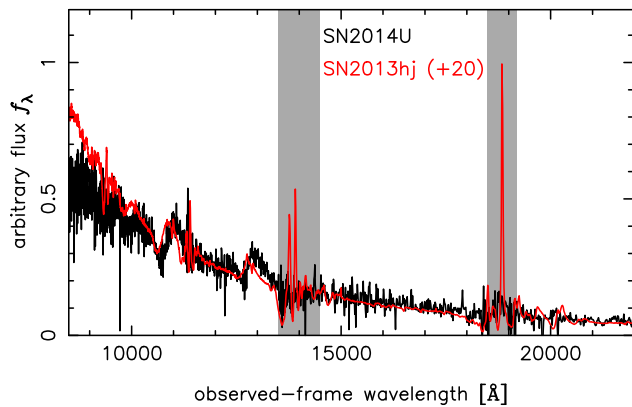
Fig. 9. Identification near-infrared spectra for SN 2014U. Flux density (f_λ) scale is in arbitrary unit. Observed and template (SN 2013hj at $t = +20$ d) spectra are shown in black and red, respectively. Telluric absorption wavelength regions are gray-shaded. (Color online)
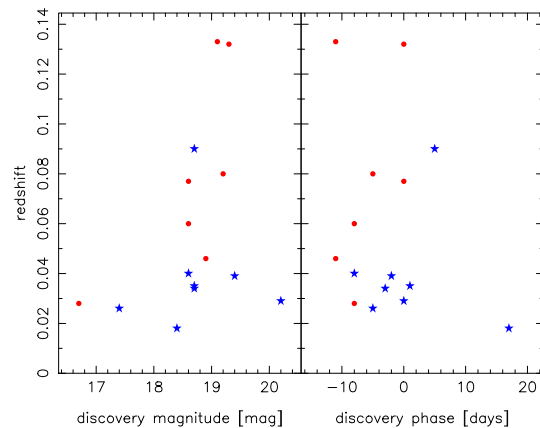
Fig. 10. Distributions of the 15 CBET-reported SNe except for SN 2014bk in discovery magnitude versus redshift in the left-hand panel and discovery phase versus redshift in the right-hand panel. SNe Ia and core-collapse SNe are shown by red circles and blue stars, respectively. (Color online)

astronomers in Japan to check whether the candidates are real astronomical sources or not and SNe or not. When we judge that a candidate is a real astronomical source and a good candidate for a newly discovered supernova, we trigger follow-up observations as described in subsection 2.3. We note that all the SNe reported in

CBET (Central Bureau Electronic Telegrams)[10] by other groups within our survey area were not missed by our reduction system.

[10] ⟨http://www.cbat.eps.harvard.edu⟩.

4 Initial results

We discovered about 80 supernova candidates up to the end of 2014 May. 16 SNe among them were spectroscopically identified within the KISS collaboration and reported to CBET. In this paper, we do not describe any details of SN 2014bk (Morokuma et al. 2014b; Stritzinger et al. 2014), a Type Ibn SN, which will be discussed in our forthcoming paper (T. Morokuma et al. in preparation). Table 2 summarizes the properties of 15 SNe (except for SN 2014bk) which include eight core-collapse SNe and seven SNe Ia. Table 3 shows a summary of spectroscopic observations for identification.

Figures 6 and 7 show the discovered KWFC images and KWFC g-band light curves of the 15 SNe. The light curve templates overplotted on the KWFC light curves for figure 7 are Nugent's templates (Nugent et al. 2002) except for a Type Ic SN (SN 2013J) for which a V-band light curve template is derived from Drout et al. (2011).[11] We do not fit the light curves with these templates, and time shifts of a few days from the spectroscopic epochs and peak magnitude shifts from the typical peak magnitudes are allowed. The absolute maximum magnitudes are also listed in table 2, which are obtained assuming the luminosity changes of the light curve templates. All the SN spectra except for that of SN 2014U are cross-correlated with a library of supernova spectra with the SNID code (Blondin & Tonry 2007) and shown in figure 8 (also except for SN 2014bk). The SN 2014U near-infrared spectrum is shown in figure 9 with the spectrum of SN 2013hj at $t = 21$ d overplotted. The spectroscopic phase t_{spec} is calculated first, from the SNID fitting results, and then the discovery epochs t_{disc} are derived from spectroscopic phase t_{spec} and time difference between the discovery and spectroscopic observations. We provide observational results for the individual SNe in the appendix. Data of these light curves and identification spectra for the 15 SNe are available on our KISS website.[12]

Apparent g-band discovery magnitudes and discovery phases t_{disc} as functions of redshift are shown in the left- and right-hand panels of figure 10, respectively. Discoveries of most of the SNe are at relatively early phases, i.e., before or around maximum light, although we have not detected shock breakouts because SNe discovered by KISS are as distant as $z > 0.02$ and only the bright parts of the SN light curves are detected. This is not unexpected because the survey volume at higher redshifts is larger. Another reason is that our observations are conducted only for $\sim$10 continuous nights around new moon and some time was lost due to bad weather. Typically our observation limits

correspond to Type Ia SNe at $z \sim 0.1$ and core-collapse SNe at $z \sim 0.04$.

The short time scale of ~ 1 hr investigated in the KISS has been a new parameter space, in which transient phenomena have not been explored enough (Ivezić et al. 2008; Kasliwal 2011). This new survey would have the potential to provide serendipitous detection of rapid variability as a by-product. For example, we actually detected a rapid flare of a radio-loud narrow-line type-1 AGN at $z = 0.840$ (Tanaka et al. 2014f), which may be similar to intra-night variability of γ-ray-loud narrow-line Seyfert 1 galaxies (Maune et al. 2013; Itoh et al. 2013).

5 Summary

We describe a new SN survey, KISS, optimized for detecting SN shock breakouts using high-cadence wide-field imaging observations with the KWFC on the 1.05-m Kiso Schmidt telescope. Based on theoretical models, we simulate observed light curves of shock breakouts and those in the plateau phases and find that the best strategy to detect, identify, and characterize shock breakouts is observations in a single bandpass, g, with a 1-hr cadence (t_{int}), five visits per night (N_{visit}), corresponding to 20 fields (N_{field}). The expected number of shock breakout detections is of the order of 1 during the three-year KISS project duration. Multi-band photometry obtained with quick follow-up observations would provide detailed information on the progenitor stars. We have developed quick automatic data reduction and image subtraction systems, including human visual screening by us and our volunteers, which would provide candidate catalogs about 15 min after the observations. We also summarize our discovery, follow-up observations and spectrum identification results for the 16 CBET-reported SNe that include nine core-collapse SNe and seven SNe Ia.

Acknowledgments

---

[11] ⟨https://www.cfa.harvard.edu/~mdrout/SN_Templates.html⟩.

[12] ⟨http://www.ioa.s.u-tokyo.ac.jp/kisohp/KISS/datarelease_en.html⟩.

Appendix. SNe discovered and reported to CBET by KISS

We note that apparent magnitudes shown in this appendix are the SN brightness measured in the daily-stacked KWFC g-band images, which are different from the brightness in our CBET reports.

(i) SN 2012cm ($g = 16.8$) was discovered on 2012 May 13.6 at (RA, Dec) ($09^h10^m05^s.45$, $+20°12'45''.1$). SN 2012cm is located $1''.2$ east and $0''.5$ south of the host galaxy, SDSS J091005.37+201245.6, at $z_{SDSS} = 0.0282$. Nothing is detected at this position on SDSS and KWFC reference or subtracted images taken on and before 2012 April 28. A spectrum taken with HOWPol on the 1.5-m Kanata telescope on 2012 May 17.5 shows clear Si II, S II, and Fe III features. Spectral fitting with the SNID code indicates that the spectrum is most similar to 4 days before maximum of a slightly overluminous Type Ia SN, SN 2002hu (Sahu et al. 2006a).

(ii) SN 2012cq ($g = 18.2$) was discovered on 2012 May 13.5 at (RA, Dec) ($09^h08^m05^s.46$, $+20°30'12''.5$). SN 2012cq is located $4''.8$ west and $0''.1$ south of the host galaxy, SDSS J090805.78+203012.6 (UGC 4792: Giovanelli et al. 1997) at $z_{SDSS} = 0.0256$. Nothing was detected at this position on the SDSS and KWFC reference or subtracted images taken on and before 2012 April 28. SN 2012cq was confirmed after discovery with the Lulin 1-m telescope and the HOWPol on the 1.5-m Kanata telescope. g-band magnitude was measured to be 18.1 on 2012 May 14.5 and 16.5. A spectrum was taken with DOLORES on the 3.5-m TNG on 2012 May 24.9. The spectrum shows a series of hydrogen Balmer features and is similar to that of a Type IIP SN, SN 2004et (Sahu et al. 2006b) 6 days after the maximum, according to the SNID code.

(iii) SN 2012ct ($g = 18.0$) was discovered SN 2012ct on 2012 May 22.5 at (RA, Dec) ($16^h32^m13^s.92$, $+38°39'25''.1$). SN 2012ct is located $2''.7$ east and $5''.1$ north of the host galaxy, SDSS J163213.74+383920.1, at $z_{SDSS} = 0.0393$. Nothing was detected at this position on reference images taken on and before 2012 May 12. A spectrum was taken with DOLORES on the 3.5-m TNG on 2012 May 24.9. The spectrum shows a series of hydrogen Balmer features indicating the SN 2012ct is a Type II SN. According to spectral fitting with the SNID, the SN 2012ct spectrum is most similar to a moderately subluminous Type IIP SN appeared in M 51, SN 2005cs (Pastorello et al. 2009) around the maximum light.

(iv) SN 2013I ($g = 18.6$) was discovered on 2013 January 11.4, at (RA, Dec) ($02^h49^m42^s.17$, $+0°45'35''.7$). SN 2013I is located $8''.8$ west and $0''.3$ south of the host galaxy, SDSS J024942.76+004535.4 at $z_{SDSS} = 0.035$. This object was also marginally detected at $g \sim 20$ in a previous image taken on 2012 November 6.6, but nothing was seen at this position in an image taken on 2012 October 21.8, or on the SDSS image. SN 2013I was also detected ($R = 17.8$) with HOWPol on the 1.5-m Kanata telescope on 2013 January 12.4. We note that SN 2013I was independently discovered by the Dark Energy Supernova Survey (DES12S1a: Brown et al. 2013). A spectrum was taken ALFOSC on the 2.5-m NOT on 2013 January 15.9. The spectrum shows multi-component Hα and Hβ emission features, superposed on a continuum containing a number of broad absorption features. According to spectral fitting with the SNID code, the SN 2013I spectrum resembles a spectrum of a Type IIP SN, SN 2005cs, around 5 days after the maximum as well as the SN 2012ct spectrum.

(v) SN 2013J ($g = 18.8$) was discovered on 2013 January 19.8 at (RA, Dec) ($11^{\rm h}12^{\rm m}50^{\rm s}\!.30$, $+28°04'19''\!.7$). SN 2013J is located $1''\!.5$ west and $5''\!.5$ north of the host galaxy (KUG 1110+283 or SDSS J111250.41+280414.2 at $z_{\rm NED} = 0.034$) (Mahdavi & Geller 2004). This object was also marginally detected at $g \sim 20$ in our previous image taken on 2013 January 15.8, but nothing is seen at this position in an image taken on or before 2013 January 12.8 or in the SDSS image. The light curve matches that of the Type Ic template in Drout et al. (2011) better than that in Nugent, Kim, and Perlmutter (2002), which is not surprising as the Drout sample is larger and more recent than the Nugent sample. A spectrum was taken with ALFOSC on the 2.5-m NOT on 2013 January 21.2. According to the spectral fitting with the SNID code, the spectrum is most similar to the maximum-light ($t \sim -2$ d) spectrum of a fast-fading Type Ic SN, SN 1994I (Filipenko et al. 1995).

(vi) SN 2013Y ($g = 18.7$) was discovered on 2013 February 6.7, at (RA, Dec) ($12^{\rm h}09^{\rm m}39^{\rm s}\!.70$, $+16°12'14''\!.3$). The SN is located $1''\!.2$ east and $2''\!.1$ north of the host galaxy, SDSS J120939.62+161212.2 at $z_{\rm SDSS} = 0.077$. Nothing is seen at this position in the SDSS image. This object was confirmed with the Swope 1-m telescope at Las Campanas Observatory. A spectrum was taken with ALFOSC on the 2.5-m NOT on 2013 February 11.2. Spectral fitting with the SNID code indicates that the spectrum is most similar to that of a very normal Type Ia SN, SN 2005cf (Garavini et al. 2007; Wang et al. 2009) at 5 days past maximum light.

(vii) SN 2013al ($g = 19.2$) was discovered on 2013 March 3.4 at (RA, Dec) ($11^{\rm h}14^{\rm m}54^{\rm s}\!.07$, $+29°35'06''\!.0$). SN 2013al is located $3''\!.0$ south of a possible host galaxy, SDSS J111454.06+293508.6. Nothing is seen at this position in an image taken on 2013 February 6.7. This object is also detected with the WIYN 0.9-m telescope at Kitt Peak at magnitudes $V = 19.4$, $R = 19.1$, and $I = 19.3$ on 2013 March 5.2. A spectrum was taken with DOLORES on the 3.58-m TNG on 2013 March 7.1. According to spectral fitting with the SNID, the best match to the spectrum of SN 2013al is the Type Ia SN, SN 2006cf at $t = +2$ d. The redshift of the host galaxy is derived from the same spectrum data and found to be $z_{\rm host} = 0.1321$ from its [O II], Hβ, [O III], and Hα emission lines of the host galaxy.

(viii) SN 2013ba ($g = 19.9$) was discovered on 2013 April 4.7 at (RA, Dec) ($13^{\rm h}52^{\rm m}56^{\rm s}\!.63$, $+21°56'21''\!.7$). SN 2013ba is located $0''\!.7$ east and $0''\!.8$ north of a

possible host galaxy, SDSS J135256.58+215620.9. Nothing is seen at this position in images taken on 2013 March 10.8. The SN was confirmed with the Swope 1-m telescope at Las Campanas Observatory. A spectrum was taken with ALFOSC on the NOT on 2013 April 7.2. According to spectral fitting with the SNID code, the SN 2013ba spectrum is most similar to that of a normal Type Ia SN, SN 1997bp (Altavilla et al. 2004) a few days before maximum light. The redshift of $z_{\rm SN} = 0.08$ is derived from the SN spectrum fitting.

(ix) SN 2014Q ($g = 19.2$) was discovered on 2014 January 29.4 at (RA, Dec) ($08^{\rm h}18^{\rm m}50^{\rm s}\!.20$, $+57°06'02''\!.9$). SN 2014Q is located $2''\!.4$ west and $2''\!.7$ south of the host galaxy, SDSS J081850.49+570605.5; $z_{\rm SDSS} = 0.046$. The SN was confirmed with the optical three-color CCD cameras on the MITSuME 50-cm telescope of the Akeno Observatory, on 2014 February 1.5. The SN was also marginally detected in a g-band KWFC image on 2014 January 27.4, but nothing is seen at this position in an image taken on 2014 January 6.5 or in the previous SDSS image. A spectrum was taken with DOLORES on the 3.58-m TNG on 2014 February 6.0. The spectrum of SN 2014Q is found to be most similar to that of a normal Type Ia SN, SN 2002he, around 3 days before maximum. Optical spectra of this object were also obtained with KOOLS on the Okayama 188-cm telescope on 2013 January 30.8 and 31.8, and the continuum was significantly detected.

(x) SN 2014S ($g = 18.8$) was discovered on 2014 February 21.5 at (RA, Dec) ($10^{\rm h}40^{\rm m}24^{\rm s}\!.98$, $+53°57'58''\!.6$). The SN is located $6''\!.6$ west and $5''\!.4$ north of the presumed host galaxy, SDSS J104025.73+535753.2. Nothing is detected at this position in an image taken on 2014 January 31.6. SN 2014S was also detected with HONIR on the Kanata 1.5-m telescope with the following magnitudes measured, $J = 18.7$ on 2014 February 22.6, $R_c = 18.4$ on 2014 February 22.6. A spectrum was taken with DOLORES on the 3.58-m TNG on 2014 February 25.1. The spectrum shows a strong blue continuum with faint emission lines of Hγ, Hδ, and He I, corresponding to a redshift of $z_{\rm SN} = 0.04$. Using the SNID code, the best matches to the spectrum of SN 2014S are to a Type IIP SN, SN 1999gi (Leonard et al. 2002) 4 days before the maximum. Due to the faint emission lines, distinguishing between a Type IIP or a Type IIn event is difficult.

(xi) SN 2014T ($g = 18.7$) was discovered on 2014 February 22.7 at a position (RA, Dec) ($14^{\rm h}36^{\rm m}04^{\rm s}\!.98$,

$+02°20'34''.2$). SN 2014T is located $1''.5$ east and $1''.6$ north of the presumed host galaxy, SDSS J143604.90+022032.6. Nothing is seen at this position in an image taken on 2013 May 9.7. A spectrum was taken with DOLORES on the 3.58-m TNG on 2014 February 25.2. The spectrum shows a blue continuum with strong emission lines of $H\alpha$, $H\beta$, $H\gamma$, and $H\delta$ and also He I at a redshift of $z_{SN} = 0.09$. Using the SNID code, many good matches to the SN 2014T spectrum are spectra of galaxies and AGNs but the best match is to the spectrum of a Type IIn SN, SN 1996L, at 8 days past explosion, based on visual inspection.

(xii) SN 2014U $(g = 18.9)$ was discovered on 2014 February 23.5 at a position (RA, Dec) $(11^h 44^m 52^s.16,$ $+19°27'17''.8)$. SN 2014U is located $1''.0$ west and $2''.8$ north of the center of the galaxy NGC 3859 at $z_{NED} = 0.01824$ (Haynes et al. 1997). Nothing is seen at this position in an image taken on 2014 January 31.8. A near-infrared spectrum was taken with the FIRE spectrograph on the 6.5-m Magellan Baade Telescope on 2014 February 27.2. The near-infrared spectrum reduced with basic methods (Hsiao et al. 2013) is similar to that of SN 2013hj at approximately 21 days past explosion with several hydrogen Paschen P-Cyg lines, indicating that SN 2014U is a Type II SN.

(xiii) SN 2014an $(g = 18.6)$ was discovered on 2014 March 31.7, at a position (RA, Dec) $(14^h 51^m 42^s.93,$ $+08°34'12''.5)$. SN 2014an is located $5''.3$ east and $15''.8$ north of the center of the galaxy SDSS J145142.57+083356.6 (CGCG 076-079) at $z_{SDSS} = 0.060$. Nothing is seen at this position in an image taken on 2014 February 24.7. This SN was confirmed to be $V = 18.9$ with the Swope 1-m telescope at Las Campanas Observatory on 2014 April 2.8. An optical spectrum of SN 2014an was taken with KOOLS on the Okayama 188-cm telescope on 2014 April 2.7. Cross-correlation with the SNID code shows that the best match is a normal SN Ia, SN 1984A, at $t = -6$ d.

(xiv) SN 2014bd $(g = 20.0)$ was discovered on 2014 April 23.6, at a position (RA, Dec) $(14^h 50^m 48^s.07,$ $+09°22'48''.3)$. SN 2014bd is located $1''.4$ west and $5''.9$ north of the center of the galaxy SDSS J145048.16+092242.3 at $z_{SDSS} = 0.029$. Nothing is seen at this position in the image taken on 2014 March 31.7. The object was confirmed with the Swope 1-m telescope at Las Campanas Observatory on 2014 April 24.2 at $r = 19.8$. An optical spectrum of SN 2014bd was obtained on 2014 May 6.3 with the WFCCD on the Las Campanas 2.5-m du Pont telescope. No order-sorting filters were used but our spectroscopic classification would not suffer due to this (Folatelli et al. 2013), which is also the case for SN 2014bd. An $H\alpha$ P-Cygni profile is seen, indicating that SN 2014bd is a type-II SN. Cross-correlation with the SNID code shows good matches with Type IIP SN around 10 days after maximum and the best match is SN 2005cs at $t = 13$ d.

(xv) SN 2014bo $(g = 19.3)$ was discovered on 2014 May 19.7, at (RA, Dec) $(16^h 27^m 46^s.15,$ $+41°44'23''.7)$. SN 2014bo is located $3''.4$ east and $5''.0$ north of the center of the host galaxy SDSS J162745.84+414418.6 at $z_{SDSS} = 0.133$. Nothing is seen at this position in an image taken on 2014 May 17.5 (limiting mag 20.0). The SN was confirmed in R-band images taken with the 0.7-m telescope at the Sternberg Astronomical Institute on 2014 May 20.9. A spectrum of SN 2014bo was taken on 2014 May 27.5 with KOOLS on the Okayama 188-cm telescope. Spectral fitting with the SNID code indicates that the best-matched template spectrum to the SN 2014bo spectrum is a normal SN Ia, SN 1994S, at 3 days before maximum. We note that the expected maximum absolute magnitude in g-band without K-correction could be as bright as -20.0, possibly indicating the overluminous nature of this SN Ia.

References

Altavilla, G., et al. 2004, MNRAS, 349, 1344

Arcavi, I., et al. 2010, ApJ, 721, 777

Baltay, C., et al. 2013, PASP, 125, 683

Barbieri, C. 1997, Exp. Astron., 7, 257

Bertin, E., & Arnouts, S. 1996, A&AS, 317, 393

Blinnikov, S., Lundqvist, P., Bartunov, O., Nomoto, K., & Iwamoto, K. 2000, ApJ, 532, 1132

Blondin, S., & Tonry, J. L. 2007, ApJ, 666, 1024

Bloom, J. S., et al. 2012, PASP, 124, 1175

Brinchmann, J., Charlot, S., White, S. D. M., Tremonti, C., Kauffmann, G., Heckman, T., & Brinkmann, J. 2004, MNRAS, 351, 1151

Brink, H., Richards, J. W., Poznanski, D., Bloom, J. S., Rice, J., Negahban, S., & Wainwright, M. 2013, MNRAS, 435, 1047

Brown, P. J., et al. 2013, Astronomer's Telegram, 4741

Cohen, S. H., et al. 2006, ApJ, 639, 731

Drake, A. J., et al. 2009, ApJ, 696, 870

Drout, M. R., et al. 2011, ApJ, 741, 97

Eastman, R. G., Woosley, S. E., Weaver, T. A., & Pinto, P. A. 1994, ApJ, 430, 300

Filippenko, A. V., et al. 1995, ApJ, 450, L11

Folatelli, G., et al. 2013, ApJ, 773, 53

Frieman, J. A., et al. 2008, AJ, 135, 338

Garavini, G., et al. 2007, A&A, 471, 527

Gezari, S., et al. 2008, ApJ, 683, L131

Giovanelli, R., Avera, E., & Karachentsev, I. D. 1997, AJ, 114, 122

Grogin, N. A., et al. 2011, ApJS, 197, 35

Harutyunyan, et al. 2008, A&A, 488, 383

Haynes, M. P., Giovanelli, R., Herter, T., Vogt, N. P., Freudling, W., Maia, M. A. G., Salzer, J. J., & Wegner, G. 1997, ApJ, 113, 1197

Hsiao, E. Y., et al. 2013, ApJ, 766, 72

Hsiao, E. Y., et al. 2014, CBET, 3816, 2

Itoh, N., et al. 2001, Pub. Nat. Astron. Obs. Jpn, 6, 41

Itoh, R., et al. 2012, CBET, 3126, 2

Itoh, R., et al. 2013, ApJ, 775, L26

Ivezić, Ž., et al. 2008, arXiv:0805.2366

Kaiser, N., et al. 2002, Proc. SPIE, 4836, 154

Kashikawa, N., et al. 2002, PASJ, 54, 819

Kasliwal, M. 2011, PhD thesis, California Institute of Technology, 35

Kawabata, K. S., et al. 2008, Proc. SPIE, 7014, 70144L

Keller, S. C., et al. 2007, Publ. Astron. Soc. Aust., 24, 1

Klein, R. I., & Chevalier, R. A. 1978, ApJ, 223, L109

Koekemoer, A. M., et al. 2011, ApJS, 197, 36

Komatsu, E., et al. 2011, ApJS, 192, 18

Konishi, M., et al. 2015, PASJ   in press

Kotani, T., et al. 2005, Nuovo Cimento C, 28, 755

Law, N. M., et al. 2009, PASP, 121, 1395

Leonard, D. C., et al. 2002, AJ, 124, 2490

Lipunov, V. M., et al. 2004, Astron. Nachr., 325, 580

Mahdavi, A., & Geller, M. J. 2004, AJ, 607, 202

Matsumoto, E., et al. 2013, CBET, 3465, 1

Maune, J. D., Miller, H. R., & Eggen, J. R. 2013, ApJ, 762, 124

Minezaki, T., et al. 2010, Proc. SPIE, 7733, 773356

Morokuma, T., et al. 2008, ApJ, 676, 163

Morokuma, T., et al. 2012a, CBET, 3126, 1

Morokuma, T., et al. 2012b, CBET, 3139, 1

Morokuma, T., et al. 2012c, CBET, 3145, 1

Morokuma, T., et al. 2013, CBET, 3414, 1

Morokuma, T., et al. 2014a, CBET, 3806, 1

Morokuma, T., et al. 2014b, CBET, 3894, 1

Morrell, N., et al. 2014, CBET, 3884, 2

Motohara, K., et al. 2010, Proc. SPIE, 7735, 77353K

Nugent, P., Kim, A., & Perlmutter, S. 2002, PASP, 114, 803

Pâris, I., et al. 2014, A&A, 563, A54

Pastorello, A., et al. 2008, MNRAS, 389, 113

Pastorello, A., et al. 2009, MNRAS, 370, 1752

Postman, M., et al. 2012, ApJS, 199, 25

Rau, A., et al. 2009, PASP, 121, 1334

Sahu, D. K., Anupama, G. C., & Prabhu, T. P. 2006a, MNRAS, 366, 682

Sahu, D. K., Anupama, G. C., Srividya, S., & Muneer, S. 2006b, MNRAS, 372, 1315

Sakimoto, K., et al. 2012, Proc. SPIE, 8446, 844673

Sako, M., et al. 2008, AJ, 135, 348

Sako, S., et al. 2008, Proc. SPIE, 7012, 70122T

Sako, S., et al. 2012, Proc. SPIE, 8446, 84466L

Sako, M., et al. 2014, ApJS   submitted (arXiv:1401.3317)

Sarajedini, V. L., et al. 2006, ApJS, 166, 69

Sarajedini, V. L., Gilliland, R. L., & Kasm, C. 2003, ApJ, 599, 173

Schawinski, K., et al. 2008, Science, 321, 223

Shimokawabe, T., et al. 2008, AIP Conf. Proc., 1000, 543

Soderberg, A. M., et al. 2008, Nature, 453, 469

Stritzinger, M. D., et al. 2013a, CBET, 3386, 2

Stritzinger, M. D., et al. 2013b, CBET, 3465, 2

Stritzinger, M. D., et al. 2014, CBET, 3894, 2

Tabur, V. 2007, Publ. Astron. Soc. Aust., 24, 189

Taddia, F., et al. 2013a, CBET, 3388, 2

Taddia, F., et al. 2013b, CBET, 3414, 2

Tanaka, M., et al. 2013a, CBET, 3386, 1

Tanaka, M., et al. 2013b, CBET, 3388, 1

Tanaka, M., et al. 2013c, CBET, 3438, 1

Tanaka, M., et al. 2014a, CBET, 3814, 1

Tanaka, M., et al. 2014b, CBET, 3815, 1

Tanaka, M., et al. 2014c, CBET, 3816, 1

Tanaka, M., et al. 2014d, CBET, 3848, 2

Tanaka, M., et al. 2014e, CBET, 3898, 2

Tanaka, M., et al. 2014f, ApJ, 793, L26

Tominaga, N., et al. 2014a, CBET, 3848, 1

Tominaga, N., et al. 2014b, CBET, 3884, 1

Tominaga, N., et al. 2014c, CBET, 3898, 1

Tominaga, N., Blinnikov, S., Baklanov, P., Morokuma, T., Nomoto, K., & Suzuki, T. 2009, ApJ, 705, L10

Tominaga, N., Morokuma, T., Blinnikov, S. I., Baklanov, P., Sorokina, E. I., & Nomoto, K. 2011, ApJS, 193, 20

Utrobin, V. P., & Chugai, N. N. 2009, A&A, 506, 829

van Dokkum, P. G. 2001, PASP, 113, 1420

Véron-Cetty, M.-P., & Véron, P. 2010, A&A, 518, A10

Villforth, C., Koekemoer, A. M., & Grogin, N. A. 2010, ApJ, 723, 737

Voges, W., et al. 1999, A&A, 349, 389

Walker, E. S., et al. 2012a, CBET, 3139, 2

Walker, E. S., et al. 2012b, CBET, 3145, 2

Walker, E. S., et al. 2013, CBET, 3438, 2

Walker, E. S., et al. 2014a, CBET, 3806, 2

Walker, E. S., et al. 2014b, CBET, 3814, 2

Walker, E. S., et al. 2014c, CBET, 3815, 2

Wang, X., et al. 2009, ApJ, 697, 380

Watson, M. G., et al. 2009, A&A, 493, 339

Wittman, D. M., et al. 2002, Proc. SPIE, 4836, 73

Yanagisawa, K., Kuroda, D., Yoshida, M., Shimizu, Y., Nagayama, S., Toda, H., Ohta, K., & Kawai, N. 2010, AIP Conf. Proc., 1279, 466

Yatsu, Y., et al. 2007, Physica E, 40, 434

Yoshida, M. 2005, J Korean Astron. Soc., 38, 117